J Mater Sci (2011) 46:2672–2677
DOI 10.1007/s10853-010-5124-x

Nanocrystalline wurtzite Si–nickel silicide composite thin films with large band gap and high resistivity

Md. Ahamad Mohiddon · M. Ghanashyam Krishna

Received: 5 October 2010 / Accepted: 29 November 2010 / Published online: 14 December 2010
© Springer Science+Business Media, LLC 2010

Abstract Stabilization of wurtzite Si nanocrystals embedded in a metal/metal silicide matrix by the metal induced crystallization process is demonstrated. The process involves the growth of 50 nm thick Ni films on borosilicate glass (BSG) substrates followed by 700 nm thick amorphous Si films and annealing of this multilayered stack at 550 °C in furnace atmosphere for 1 h. The presence of wurtzite Si is established based on electron diffraction studies and is also confirmed by the Raman signature of wurtzite Si at 504 cm^{-1}. It is shown that the growth of wurtzite Si is mediated by the formation of Nickel Silicide, as evidenced by the Raman signal at 294 cm^{-1}. The films exhibit a band gap greater than 1.9 eV with dc resistances of the order of 10 GΩ. It is proposed that such high resistivities should make this form of Si ideal for PV and microwave device applications.

Introduction

Silicon (Si) usually crystallizes in the cubic diamond structure with fourfold coordinated symmetry. Numerous high-pressure experiments have been performed, revealing no less than 12 different polymorphs of silicon between the well characterized diamond cubic phase and theoretically intractable amorphous phase. With the release of pressure several metastable phases are observed [1, 2]. For example, a nonmetal to metal transition from the ambient pressure cubic-diamond phase occurs at 10^{-13} GPa to form a β-tin structure, which transforms on slow pressure release to a rhombohedral phase. The latter transforms reversibly at a pressure of 2 GPa to a body-centered-cubic phase (bc8). Hexagonal-wurtzite silicon (*w*-Si) can be formed by heating the bc8 phase to above 200 °C, or directly from the cubic-diamond phase in the presence of shear stresses at twin intersections [3], or a non-hydrostatic stress of 8 GPa in indentation experiments [4, 5]. *w*-Si material is rarely studied by spectroscopic measurements, because it cannot be obtained in a stable phase. Zhang et al. [6] produced stable *w*-Si phase by laser ablation. Its identification by electron diffraction has been confirmed by micro Raman spectroscopy. Bandet et al. [7] deposited *w*-Si during elaboration of SiO_2 thin films and reported that oxygen seems to play a crucial role in the stabilization of the uncommon metastable structure. Kim et al. [8] reported that, the micrometer-sized diamond cubic silicon (*c*-Si) crystals contain minority part of hexagonal silicon, when *a*-Si films crystallized by a pulsed laser. In this study the authors have crystallized the silicon film with a metal contact, which is well known as metal-induced crystallization (MIC) and found that silicon nanocrystals are in wurtzite phase. In MIC, metals like Pd, Ni, Al, Ag, Au, etc. when contact with Si, will act as a seed layer for crystallization and lower the crystallization temperature and anneal times. Among the metals employed for the study of the MIC of amorphous silicon (*a*-Si), [9, 10] the preferable metal up to date has been the nickel (Ni) due to its low residual metal contamination in the poly-Si region [11]. It is also found that good performance MIC TFT's can be obtained when Ni is employed in the MIC process. In the previous study, a preliminary study of the stabilization of wurtzite Si by Cr MIC process was reported [12]. In this study Ni-induced crystallization of amorphous Si (a-Si)

Md. A. Mohiddon (✉) · M. G. Krishna
School of Physics, University of Hyderabad, Hyderabad 500046, India
e-mail: ahamed.vza@gmail.com

M. G. Krishna
e-mail: mgksp@uohyd.ernet.in

films is reported. The stabilization of Si in the wurtzite structure is established based on Transmission electron microscopy and Raman spectroscopy evidence. The films were characterized for optical and dc resistivity behavior and it is shown that they have large band gap and high resistivity.

Experimental

Nickel and Silicon films were deposited by electron beam evaporation on to BoroSilicate Glass (BSG) substrates in high vacuum of the order of 10^{-6} Torr. In all cases the substrate to source distance was kept constant at 10 cm. The starting materials were granular pure silicon powder (99.999%) and nickel powder (99.99% pure). First a 50 nm thin nickel blanket bottom layer was deposited on BSG substrates maintained at ambient temperature. This is followed by the deposition of a 700 nm thick Si film, without breaking vacuum, to form a BSG/Ni/Si stack.

The thickness of the films is measured after deposition using a surface profilometer (model XP-1 Ambios Tech., USA). The films were annealed in a furnace atmosphere (in air) at 550 °C for 1 h. Before and after annealing, the films were characterized for transmission in the wavelength range 200–2400 nm by means of a dual-beam spectrophotometer (UV–vis–NIR, model, Jasco V-570) having a resolution limit of ±0.2 nm and a sampling interval of 2 nm. The surface morphology of the films was examined by atomic force microscopy (AFM) (SPA 400 of Seiko Instruments Inc., Japan with SPI-3800 probe station). Transmission electron micrographs were obtained by a Tecnai 20 G2 STwin, FEI electron microscope, operated at 200 kV. Electron diffraction patterns (EDPs) were recorded with a Gatan CCD camera. A 10 nm gold film deposited on the grid was used for camera length calibration purposes. The Raman spectra were recorded in air using an Nd-YAG 532 nm laser in the back scattering geometry in a CRM spectrometer equipped with a confocal microscope and 100× objective (1 μm diameter focal spot size) with a CCD detector (model alpha 300 of WiTec Germany). The phase content with in the samples was investigated in a spectral region 200–1500 cm^{-1}. For DC resistance measurements we have coated film as BSG/Si/Ni to investigate the diffusion of Ni layer into Si layer. DC resistivity measurements were made using a standard two probe geometry.

Results and discussion

Figure 1a shows the electron diffraction pattern along with a bright-field transmission electron micrograph obtained from a region in the silicon thin film crystallized by a MIC process in the inset. The typical microstructure shown in inset of Fig. 1a consists of spherical particles with approximate diameter of 40 nm. The diffraction spots can be identified as belonging to well defined orientations. The calculated interplanar distances of the lattice planes at different spots of the diffraction pattern assigned by symbols A, B, and C in Fig. 1 are A = 0.256, B = 0.237, and C = 0.237 nm, respectively. From the calculated interplanar distances the diffraction spots were indexed as (1 0 0), (1 $\bar{1}$ 1), and (O $\bar{1}$ 1), which belong to the [1$\bar{2}$13] zone axis. These diffraction spots were diffracted from a grain which has a hexagonal structure and oriented in the [1$\bar{2}$13] direction and the spots A, B, and C were diffracted from the (1 0 0), (1 $\bar{1}$ 1), and (O $\bar{1}$ 1) planes, respectively.

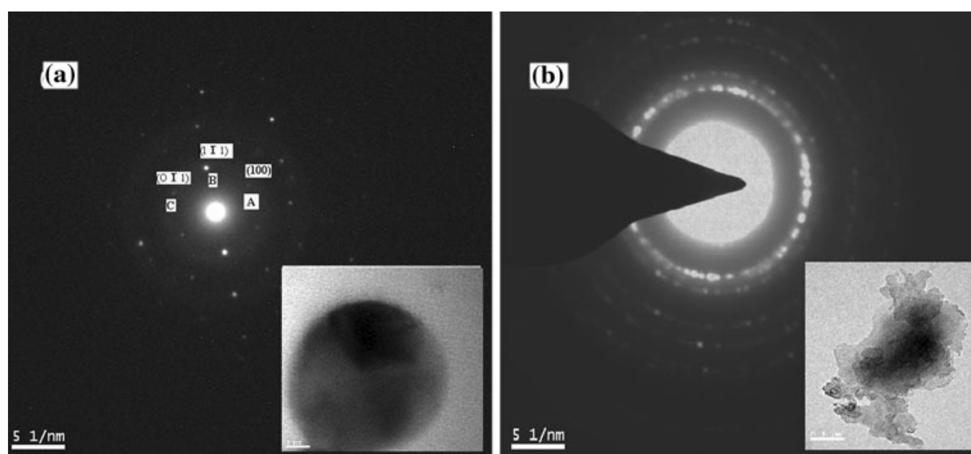

Fig. 1 Electron diffraction pattern along with indexing of selected *w*-Si part of BSG/Ni/Si stack annealed at 550 °C for 1 h, *inset* shows the bright field image of the above diffraction area, **b** Electron diffraction pattern of selected $NiSi_2$ part of BSG/Ni/Si stack annealed at 550 °C for 1 h, *inset* shows the bright field image of the above diffraction area

The corresponding lattice parameters were calculated as $a = 0.296$ nm, $c = 0.629$ nm with c/a ratio of 2.13. The angle calculated between these planes using c/a value is found to be exactly matching with the measured values suggesting that Si crystallizes in the hexagonal structure. For diamond cubic Si crystals the interplanar distances of the lattice planes should be 0.33 1, 0.33 1, and 0.331 nm, respectively and the angles between transmitted beam and the spots will be 60°, 60°, and 60°, with the diffraction pattern showing the expected six fold symmetry. But in this case the angles between the dots are $\angle AOB = 65°$, $\angle BOC = 55°$, and $\angle AOC = 120°$, respectively, clearly not cubic Si. Figure 1b shows the TEM diffraction pattern of another part of the same sample whose bright field image is shown in the inset of the figure. The inset shows a cluster of particles whose diffraction pattern consists of polycrystalline rings. The calculated interplanar spacings are 0.197, 0.171, 0.115, and 0.103 nm, respectively. Due to the very bright spot of direct beam, the closest 0.312 nm ring is not visible in the image. This polycrystalline ring pattern may belong either to face centered cubic phase of $NiSi_2$ or diamond cubic Si phase. From the ratio of the square of the radii of the rings it was determined that the diffraction pattern fits to a face centered cubic structure (1,3,4,8,11,12…) rather than the cubic phase of Si. Hence it is confirmed that the polycrystalline diffraction pattern belongs to $NiSi_2$. The rings are indexed as corresponding to the (220), (311), (422), and (440) planes with the central ring attributed to the (111) plane. Thus, the TEM analysis shows that the BSG/Ni/Si stack after heat treatment consists of 40 nm particles of hexagonal Silicon with c/a ratio of 2.11 along with polycrystalline $NiSi_2$.

Additional evidence for the formation of *w*-Si is provided in the form of Raman spectra of the films. It has earlier been used to characterize porous Si [13] and Si nanostructures [14]. The Raman shift and the shape of the Raman peak yield information on the degree of crystallinity achieved in Si by MIC process. Figure 2a shows Raman spectra from the Silicon film annealed at 550 °C for 1 h. A sharp peak at 504 cm^{-1} and weak broad peaks around 300 and 950 cm^{-1}, are associated with optical phonons, two transverse acoustic (2TA) phonons, and two transverse optical (2TO) phonons of *w*-Si, respectively [1, 2, 15, 16]. The asymmetric nature of the peak at 504 cm^{-1} can be attributed to the presence of small amounts of *a*-Si, which has its broad peak at 480 cm^{-1}. In general, when Si crystallizes in cubic diamond structure the Raman peak occurs at 520 cm^{-1}. NiSi phase has two relatively strong Raman peaks at 195 and 214 cm^{-1} with minor peaks at 258, 294, and 362 cm^{-1} [17]. Due to cubic structure of $NiSi_2$, there are no symmetry allowed first order Raman peaks, consequently all the other vibrational peaks (232, 297, 320, 402 cm^{-1}) are weak and broad [18–20]. So the broad peaks around 283 cm^{-1} in the observation is may belong to NiSi, $NiSi_2$ or to wurtzite TA mode. However, this observation implies that, at 550 °C nickel silicides are present in the samples. Figure 2b and c show Raman images mapped for *w*-Si and $NiSi_2$ distribution across a 5 × 5 micron area of sample scanned by selecting a particular part of spectrum [(a)500–510 cm^{-1}, which belong to *w*-Si, (b) 250–320 cm^{-1} a very broad peak of NiSi, $NiSi_2$ and *w*-Si]. The bright area in the figure shows the Si rich area of selected part of the spectrum. As discussed above a broad peak around 280 cm^{-1} could be due to NiSi, $NiSi_2$ and acoustic phonon modes of *w*-Si. These maps confirm that the peak around 280 cm^{-1} is not from *w*-Si but has a major contribution from $NiSi_2$. Furthermore, Fig. 2b shows the distribution of *w*-Si is not uniform throughout the area. In contrast, Fig. 2c shows that the signal around 280 cm^{-1} peak is uniform across the maximum part of scanned area. These observations suggest that $NiSi_2$, act as seed for crystallization of Si, and eventually moves away from the crystallization centre leaving *c*-Si.

Tan et al. [21] reported a stress-induced metastable form of hexagonal silicon, which has the wurtzite structure with the c/a ratio close to 1.63, the interplanar distances and

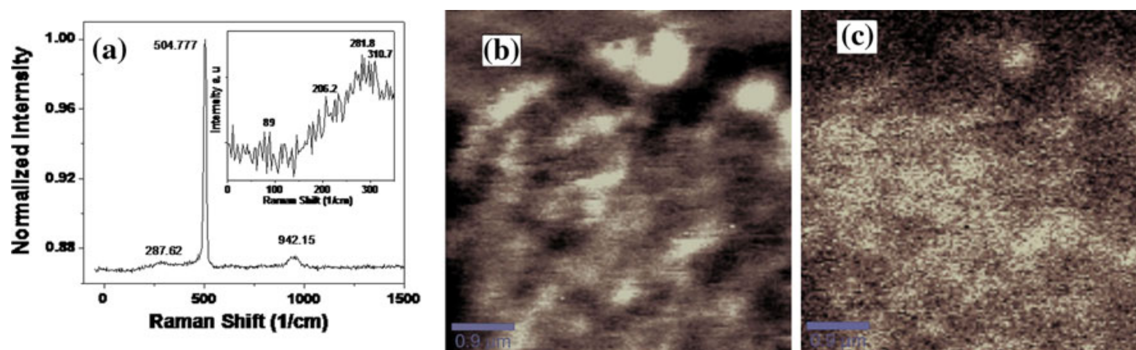

Fig. 2 **a** Raman spectra of BSG/Ni/Si stack annealed at 550 °C for 1 h; **b** Raman mapping of (a) *w*-Si, (filter selected for 500–510 cm^{-1}) **c** $NiSi_2$ (filter for 250–320 cm^{-1}) across a selected 5 × 5 micron area of the BSG/Ni/Si stack annealed at 550 °C for 1 h

angular relationships obtained from our experiment were compared with those of silicon which has the wurtzite structure. However, for silicon with the wurtzite structure, no exact coincidence was obtained. Kim et al. reported a similar observation and suggested a hexagonal phase of Si with $a = 0.382$, $c = 1.024$ nm and c/a ratio of 2.68 [22]. Parson and Hoelke suggested similar hexagonal structure for Ge with c/a ratio of 2.17 [23, 24]. Zhang et al. [25] have reported wurzite silicon by laser ablation, and they observed Raman peaks at 516 and 518 cm^{-1} due to the hexagonal silicon. Kumar et al. [12] observed *w*-Si in chromium-induced Si crystallization evidenced by a peak at 495 cm^{-1}. Kailer et al. [4] performed indentation Raman investigations and reported that, shear deformation leads to *w*-Si phase formation. They also stated that high pressure phases leads to the formation of *w*-Si at moderate temperatures and to the reversal to the original diamond structure at higher temperatures. In a very detailed and interesting study, Zhang et al. [26] have investigated the stability of polycrystalline and wurtzite Si nanowires via symmetry-adapted tight-binding objective molecular dynamics. They have also shown, from ab initio calculations, that nanocrystalline ($\sim$10 nm or less diameter) wurtzite wires of threefold symmetry in addition to achiral polycrystalline of fivefold symmetry are the most favourable quasi-one-dimensional Si arrangements.

It appears that the mechanism of crystallization of *a*-Si in the present case involves the following sequence: 1. Diffusion of Ni into *a*-Si; 2. Reaction of Ni with Si to form a Silicide; 3. Growth of Si nanocrystals on the Silicide seeds; 4. Movement of the silicide seeds away from the crystallization front, and 5. Formation of Si nanocrystals in a silicide matrix.

Measured spectral transmittance has been shown to be an extremely useful tool to probe the process of MIC [27]. Figure 3a shows the measured spectral transmittance data over the wavelength range from 200 to 2400 nm for the as deposited as well as annealed films. The spectra in both cases can be divided into regions of high transmission where interference fringes occur and the region of band gap with low transmission, high absorption and no interference fringes. The height of the fringes is a measure of the refractive index while their width relates to the thickness of the film [28]. The absolute values of transmission give an indication of the optical losses in the films due to absorption and scattering. The band gap is estimated from the calculated absorption coefficient in the short wavelength region. It is evident from these figures that the height of the fringes decreases on annealing indicating a decrease in the refractive index. This is accompanied by a decrease in transmittance signifying an increase in optical losses on annealing. The decrease in transmittance after heat treatment can be attributed to the formation of $NiSi_2$. Reflectance spectra for the same films are shown in the inset of Fig. 3a. A remarkable increase in reflectance was observed after heat treatment at 550 °C for 1 h. The sum of transmittance [shown in Fig. 3a] and reflectance [inset of Fig. 3a] at any wavelength, for the annealed films, is less than unity indicating the presence of absorption. This observation strongly supports our argument that after heat treatment, the Ni which is at the bottom diffuses through Si and reaches the surface in the form of silicide that causes increase in optical absorption. This is also in conformity with the observations made in the Raman spectra discussed earlier.

Refractive index (n), absorption coefficient (α) and average thickness (d) were calculated from the measured spectral transmission curves (Fig. 3a) using the envelope technique [28]. Figure 3b shows the variation of refractive index as a function of wavelength for before and after annealed sample and is observed that the refractive index decreases with increase in wavelength at short wavelengths and then becomes wavelength independent as expected of normal dispersion behavior. $dn/d\lambda$ was calculated between 800 and 1200 nm which is above the absorption edge where $dn/d\lambda$ changes rapidly, and is found to be -1.6×10^{-3} and -1×10^{-3} for the film before and after annealing. This decrease in $dn/d\lambda$ suggests increase in long-range order and hence crystallization of *a*-Si after heat treatment. Furthermore, a decrease in refractive index from 2.13 to 1.85 (at 1 μm) is observed with heat treatment. It may be noted that *a*-Si films show refractive indices of the order of 3.5 to 4.0. The lower values in the as deposited case, here, are due to the presence of the thin layer of Ni underneath the Si layer. On annealing, the refractive index is that of the composite of Si and Nickel Silicide which is lower than that of pure crystalline Silicon. Similar observations were reported in the previous study [27]. The optical absorption edge (E_g) was calculated by extrapolating the linear portions of the $(\alpha h\nu)^{1/2}$ versus $h\nu$ curve to $(\alpha h\nu)^{1/2} = 0$ [27] as shown in the Fig. 3c. The calculated E_g was 1.92 and 1.96 eV before and after annealing. These are much larger than that for pure Si and closer to that of *a*-Si:H. However, no evidence for the presence of hydrogen was found in our case. Evidently this is due to quantum confinement as a consequence of the small crystallite sizes.

The AFM images of the surface of Si thin film deposited on a BSG substrate taken before and after annealing at 550 °C for 1 h respectively are shown in Fig. 4. The morphology is homogeneous, dense and crack free, the mean surface grain size of thin film is found to be 187 and 155 nm before and after annealing, respectively.

Figure 3d shows the d.c resistance of the films as a function of annealing temperature. For this measurement, the stack geometry was BSG/Si/Ni which was then subjected to heat treatment from 100 to 500 °C in steps of

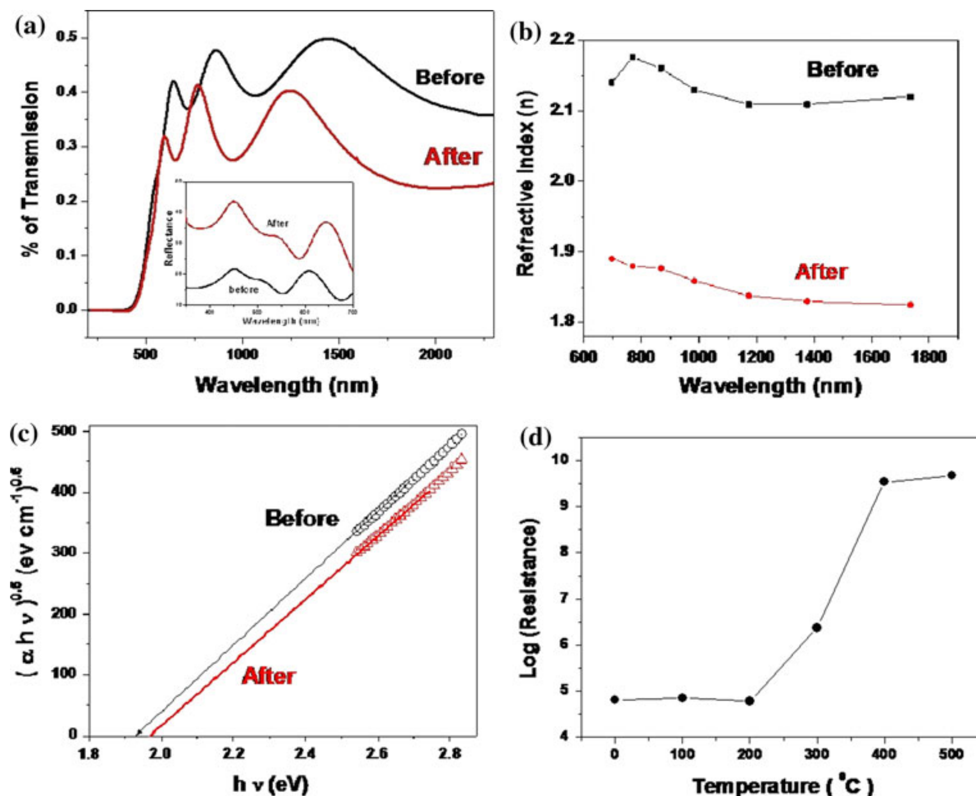

Fig. 3 **a** Measured spectral transmittance curves of BSG/Ni/Si stack before and after heat treatments along with Reflectance spectra before and after annealing in inset **b** The dispersion in refractive index as a function of wavelength. **c** The plot of the variation of $(\alpha h\nu)^{1/2}$ versus $h\nu$ for the BSG/Ni/Si stack before and after annealing. **d** Variation of d.c resistance on log scale as function of annealing temperature for BSG/Si/Ni stack

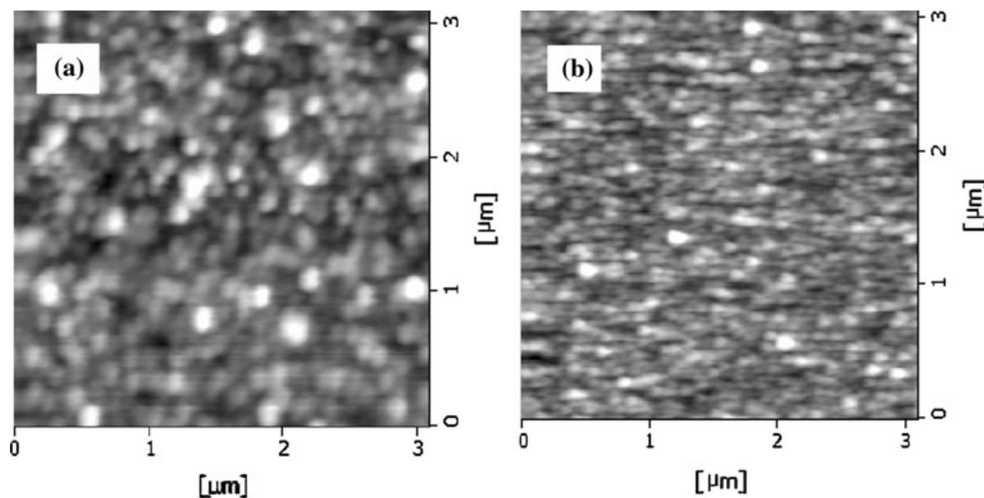

Fig. 4 AFM image of BSG/Ni/Si stack before and after heat treatment of 550 °C for 1 h

100 °C, each for 1 h. Up to 200 °C the resistance was in the KΩ range which rather dramatically increased to a few MΩ at 300 °C and finally to GΩ at 400 and 500 °C. This observation strongly supports the argument that as annealing temperature increases, Ni reacts with Si and forms nickel silicide, which diffuses into *a*-Si resulting in its crystallization. The diffusion and reaction evidently occur at temperatures >200 °C causing a large increase in the resistance. Further increase in temperature results in diffusion of silicide and the transport of polycrystalline silicon to the surface, causing the resistance to increase into the GΩ range. Such large dc resistivities make this form of Si particularly attractive as an alternate to high resistivity Si. Further studies in this direction are being carried out and will be reported elsewhere.

Conclusions

The wurtzite form of Si has been stabilized in a nickel silicide matrix by the metal-induced crystallization process of a-Si thin films. Raman spectroscopy and TEM evidence

unambiguously establishes the formation of hexagonal Si. The Si-silicide nanocomposite exhibits large band gap and high resistivity that makes this material very interesting for optoelectronic, PV and microwave applications.

Acknowledgements The authors acknowledge funding from the DST-ITPAR programme for this study, especially fellowships for MAM. Facilities provided under the DST Centre for Nanotechnolgy and UGC-CAS and UPE programmes of the School of Physics are gratefully acknowledged.

References

1. Wu BR (2000) Phys Rev B 61:5
2. Gogotsi Y, Baek C, Kirscht F (1999) Semicond Sci Technol 14:936
3. Dahmen U, Hetherington CJ, Pirouz P, Westmacott KH (1989) Scr Metall 23:269
4. Kailer A, Gogotsi YG, Nickel KG (1997) J Appl Phys 81:3057
5. Pirouz P, Chaim R, Dahmen U, Westmacott KH (1990) Acta Metall Mater 38:313
6. Zhang Y, Iqbal Z, Vijayalakshmi S, Grebel H (1999) Appl Phys Lett 75:2758
7. Bandet J, Despax B, Caumont M (2000) J Phys D Appl Phys 35:234
8. Kim JH, Lee JY (1996) Mater Lett 27:275
9. Jin Z, Moulding K, Kowk HS, Wang M (1999) IEEE Trans Electro Device 46:78
10. Hultman L, Robertson A, Hentzell HT, Engsstrom I, Psaras PA (1987) J Appl Phys 62:3647
11. Wang M, Wong M, Trans IEEE (2001) Electron Devices 48:1655
12. Kumar KU, GhanashyamKrishna M (2008) J Nanomaterials 2008:1
13. Sui Z, Leong PP, Herman IP, Higashi GS, Temkin H (1992) Appl Phys Lett 60:2086
14. Kozlowski F, Petrova-Koch V, Kux A, Stadler W, Fleischmann A, Sigmund H (1991) J Non-Cryst Solids 137:91
15. Kobliska RJ, Solin SA (1973) Phys Rev B 8:3799
16. Gribb AA, Banfield JF (1997) Am Mineral 82:717
17. Sasaki T, Nishibe S, Harima H, Isshiki T, Yoshimoto M (2006) 14th IEEE International Conference on Advanced Thermal Processing of Semiconductors 217
18. Rodriguez AP, Roca E, Jawhari T, Morante JR, Schreutelkamp RJ (1994) Thin Solid Films 251:45
19. Lee PS, Mangelinck D, Pey KL, Shen ZX, Ding J, Osipowicz T, See A (2000) Solid-State Lett 3:153
20. Zhang XW, Wong SP, Cheung WY (2002) J Appl Phy 92:3778
21. Tan TY, Foll H, Hu SM (1981) Philos Mag A 44:127
22. Kim JH, Lee JY (1996) Mater Lett 27:275
23. Parsons JR, Hoelke CW (1983) Nature 30:591
24. Parsons JR, Hoelke CW (1984) Phil Mag A 50:329
25. Zhang SL, Wang X, Ho K, Li JJ, Diao P, Cai S (1994) J Appl Phys 76:3016
26. Zhang DB, Hua H, Dumitrica T (2008) J Chem Phys 128:0841041
27. Mahendra Kumar KU, Brahma R, Ghanashyam Krishna M, Bhatnagar AK, Dalba G (2007) J Phys 19:49620801
28. Swanepoel R (1983) J Phps E 16:1214